

cy.2



MIXED FREE AND FORCED CONVECTION COOLING IN A LONG SLENDER TUBE WITH INLET EFFECTS

VON KÁRMÁN GAS DYNAMICS FACILITY
ARNOLD ENGINEERING DEVELOPMENT CENTER
AIR FORCE SYSTEMS COMMAND
ARNOLD AIR FORCE STATION, TENNESSEE 37389

December 1975

Final Report for Period February 74 — July 74

Approved for public release; distribution unlimited.

Approved for public release; distribution unlimited.

Prepared for

DIRECTORATE OF CIVIL ENGINEERING (DE)
ARNOLD ENGINEERING DEVELOPMENT CENTER
ARNOLD AIR FORCE STATION, TENNESSEE 37389

NOTICES

When U. S. Government drawings specifications, or other data are used for any purpose other than a definitely related Government procurement operation, the Government thereby incurs no responsibility nor any obligation whatsoever, and the fact that the Government may have formulated, furnished, or in any way supplied the said drawings, specifications, or other data, is not to be regarded by implication or otherwise, or in any manner licensing the holder or any other person or corporation, or conveying any rights or permission to manufacture, use, or sell any patented invention that may in any way be related thereto.

Qualified users may obtain copies of this report from the Defense Documentation Center.

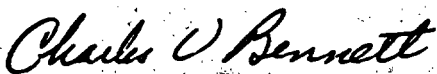
References to named commercial products in this report are not to be considered in any sense as an endorsement of the product by the United States Air Force or the Government.

This report has been reviewed by the Information Office (OI) and is releasable to the National Technical Information Service (NTIS). At NTIS, it will be available to the general public, including foreign nations.

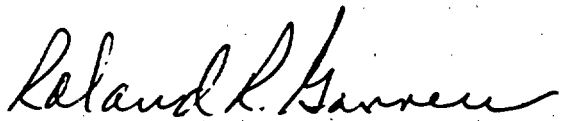
APPROVAL STATEMENT

This technical report has been reviewed and is approved for publication.

FOR THE COMMANDER



CHARLES V. BENNETT
Facility Development
Division
Directorate of Civil Engineering



ROLAND R. GARREN
Colonel, USAF
Director of Civil Engineering

UNCLASSIFIED

REPORT DOCUMENTATION PAGE		READ INSTRUCTIONS BEFORE COMPLETING FORM
1. REPORT NUMBER AEDC-TR-75-142	2. GOVT ACCESSION NO.	3. RECIPIENT'S CATALOG NUMBER
4. TITLE (and Subtitle) MIXED FREE AND FORCED CONVECTION COOLING IN A LONG SLENDER TUBE WITH INLET EFFECTS		5. TYPE OF REPORT & PERIOD COVERED Final Report-February 1974 - July 1974
7. AUTHOR(s) Frederick L. Shope, ARO, Inc.		6. PERFORMING ORG. REPORT NUMBER
9. PERFORMING ORGANIZATION NAME AND ADDRESS Arnold Engineering Development Center(DE) Arnold Air Force Station, Tennessee 37389		10. PROGRAM ELEMENT, PROJECT, TASK AREA & WORK UNIT NUMBERS Program Element 63723F
11. CONTROLLING OFFICE NAME AND ADDRESS Arnold Engineering Development Center (DYFS) Arnold Air Force Station, Tennessee 37389		12. REPORT DATE December 1975
14. MONITORING AGENCY NAME & ADDRESS (if different from Controlling Office)		13. NUMBER OF PAGES 35
		15. SECURITY CLASS. (of this report) UNCLASSIFIED
16. DISTRIBUTION STATEMENT (of this Report) Approved for public release; distribution unlimited.		15a. DECLASSIFICATION DOWNGRADING SCHEDULE N/A
17. DISTRIBUTION STATEMENT (of the abstract entered in Block 20, if different from Report)		
18. SUPPLEMENTARY NOTES Available in DDC		
19. KEY WORDS (Continue on reverse side if necessary and identify by block number) <div style="display: flex; justify-content: space-between;"> <div> convection (free, forced) cooling tube (long, slender) inlet </div> <div> boundary layer heat transfer atmospheres temperature (spatial, timewise) </div> </div>		
20. ABSTRACT (Continue on reverse side if necessary and identify by block number) <p>Results are presented concerning an experimental study of mixed free and forced convection cooling of a long slender tube where the inlet is a high-speed jet which severely disrupts the normally expected boundary layer or free convection development. The similarity parameter Gr/Re^2 ranged from 10 to 100, which would suggest free convection dominance were it not for the inlet jet. In contrast to most heat-transfer experiments, the tube was</p>		

UNCLASSIFIED

UNCLASSIFIED

20. ABSTRACT (Continued)

insulated from its external environment and its temperature was allowed to vary axially, circumferentially, and temporally in order to study the gradients induced in the tube by the free-forced convection process. The resulting rate of cooling of the tube was measured. Timewise and spatial temperature variation of both the tube and cooling air are presented for various pressure levels up to 28 atmospheres at nominally constant flow rates of 0.3 to 0.4 lb/sec. Heat-transfer coefficients derived from these data are found to be two to five times greater than anything expected from the classical Nusselt number relations. A physical model based on buoyant effects opposed by a convected decaying jet turbulence is correlated with the experimental results.

UNCLASSIFIED

PREFACE

The study presented herein was conducted by the Arnold Engineering Development Center (AEDC), Air Force Systems Command (AFSC), under Program Element 63723F. This work was done by ARO, Inc., (a subsidiary of Sverdrup & Parcel and Associates, Inc.), contract operator of AEDC, AFSC, Arnold Air Force Station, Tennessee. The research, conducted under ARO Project Number V37A-32A, was done in support of the High Reynolds Number Wind Tunnel (HIRT) Project. The author of this report was Frederick L. Shope, ARO, Inc. The manuscript (ARO Control No. ARO-VKF-TR-75-72) was submitted for publication on March 17, 1975.

The author wishes to acknowledge the contributions of Rogers F. Starr who carefully supervised and steered the effort and made many contributions to the experiment as well as the theory.

CONTENTS

	<u>Page</u>
1.0 INTRODUCTION	5
2.0 APPARATUS	6
3.0 PROCEDURE	8
4.0 RESULTS	9
5.0 DISCUSSION	18
6.0 SUMMARY OF RESULTS	20
REFERENCES	21

ILLUSTRATIONS

Figure

1. Schematic of Experimental Apparatus	7
2. Steel Temperature as a Function of Time for Run No. 2 (150 psig)	10
3. Air Survey Temperatures for Run No. 1 (400 psig)	11
4. Circumferential Steel Temperature Distribution for Run No. 1 (400 psig)	12
5. Air Survey Temperatures for Run No. 2 (150 psig)	13
6. Air Survey Temperatures for Run No. 3 (75 psig)	14
7. Dissipation of Circumferential Temperature Gradients in Tube Following Shutdown of Cooling Air	15
8. Effect of Stratification for Run No. 5 (75 psig)	15
9. Effect of Stratification for Run No. 6 (150 psig)	16
10. Steel Temperature at Top of Tube versus Axial Station for Run No. 4 (150 psig) before and after Staging	16
11. Difference between Top and Bottom Steel Temperatures for Run No. 4 (150 psig)	17
12. Experimental Heat-Transfer Coefficients Compared with Classical Nusselt Number Relations	18

TABLES

1. Tube Characteristics	6
2. Test Conditions	9

APPENDIXES

A. COMPUTATION OF HEAT-TRANSFER COEFFICIENTS FROM EXPERIMENTAL TEMPERATURE DISTRIBUTIONS	23
B. PARTIAL MODEL OF THE HEAT-TRANSFER PROCESS	25
NOMENCLATURE	33

1.0 INTRODUCTION

This study was part of the effort to develop a transonic, high Reynolds number wind tunnel (HIRT) based on the Ludwig tube concept. The proposed HIRT Facility (Ref. 1) consisted of a long slender pressure bottle (15-ft-diameter by 1,660-ft-long) which would provide high-pressure (500-psi stagnation) and low-temperature (-60°F stagnation) air to a porous walled, transonic test section. To achieve these stagnation conditions in the test section during a tunnel run, the air in the supply tube would have to be compressed to 700 psi and cooled to -30°F. In order for the charge air to remain at the desired temperature until a tunnel run could be made, the steel supply tube itself would have to be cooled to -30°F. In addition, the cooling would have to be accomplished in a reasonable length of time, and the final temperature distribution would have to be uniform (within 5°F). One proposed system to achieve these conditions would consist of a series of compressors and refrigeration units to recirculate very cold air (-60°F to -80°F) through the supply tube to cool it by forced convection. However, the flow rates (<200 lb/sec) practically attainable from reasonably sized compressors and the high pressures (~700 psi) required to avoid inordinately large recirculation and refrigeration plumbing would also result in very low bulk tube velocities and large densities. Hence, the flow could well be dominated by free convection and induce unacceptably large temperature gradients in the tube. In addition, the size of the compressors and refrigeration units would have a first order impact upon the total facility cost. Therefore, the current work was undertaken to determine if the supply tube could be suitably cooled by simply circulating cold air from one end to the other.

This report documents the results of a study of internal convection cooling of a long slender tube in which the classical free and forced convection heat-transfer mechanisms were severely disrupted by a high-speed inlet jet. The flow regime of the test corresponded to a tube diameter Reynolds number of 4×10^4 and Grashof numbers varying from 10^9 to 10^{10} ($Gr_D/Re_D^2 \sim 10$ to 100). These values resulted from relatively low velocities, approximately 0.2 to 0.7 ft/sec, and high pressures 6 to 28 atmospheres.

The experiment was performed using a steel tube about 1-in. thick, 111 feet long, and 14-in. ID. Exact dimensions are listed in Table 1. Air, cooled to between -5°F and 20°F by Joule-Thompson expansion from a 4,000-psi air supply, was injected into one end of the tube through a relatively high-speed jet (200 to 300 ft/sec) normal to the axis of the tube. Data collected included the axial and circumferential timewise temperature distributions in the steel tube and the axial and vertical timewise temperature distributions of the air.

Two things make the current experiment somewhat unique among heat-transfer tests. First, the relatively high pressures and low bulk velocities place the physical situation

at the extremes of the Reynolds number and Grashof number regimes usually covered by the classical heat-transfer experiments. However, the low Reynolds numbers result not from high viscosity, as in the oil-flow experiments, but from low velocities, and the high Grashof numbers from high pressure rather than size of the apparatus. A second unique characteristic of this experiment is that the tube was insulated from the environment and its temperature was allowed to change locally in accordance with the heat transfer required by the fluid flow. This is in contrast to the classical experiments where the tube is usually provided an external energy source to keep it at a constant temperature. Allowing the tube temperature to vary temporally and spatially is, of course, necessary in studying the development of temperature gradients.

The report documents the experimental apparatus, test procedure, data reduction and interpretation, analysis, and conclusions. Details of the data reduction and modeling are given in the Appendixes.

2.0 APPARATUS

The experimental apparatus was adapted from the supply tube of the pilot HIRT in the von Kármán Gas Dynamics Facility (VKF) (Ref. 1). The characteristics of the tube are listed in Table 1. To prepare the tube for the test, it was disconnected from the test section, though a short (18.5-in.) piece of the contraction section (a converging nozzle) was left attached to the tube in order to use an existing blind flange to seal the pressure vessel. To measure the temperature-time histories and spatial distributions in the tube steel, the tube was initially instrumented with 18 thermocouples as illustrated in Fig. 1 (open squares). At each of three stations along the tube, seven thermocouples were installed as shown in Section AA. Five copper-constantan thermocouples were spaced uniformly on the outside of the tube, and one was potted into a hole in the tube to measure inside surface temperature. In addition, at each of these three stations, a Chromel[®]-constantan thermocouple on the end of a vertically sliding tube was installed to measure vertical gradients in the air.

Table 1. Tube Characteristics

Length	111 ft
Inside diameter	13.94 in.
Thickness	1.026 in.
Density	0.283 lbm/in. ³
Specific heat	0.11 Btu/lbm
Thermal conductivity	27 Btu/hr-ft-°R
Inside roughness	0.0004-in. to 0.0007-in. roughness superimposed on a larger scale 0.001-in. to 0.0015-in. roughness of more or less flat plateaus and valleys (~0.25 in. across)

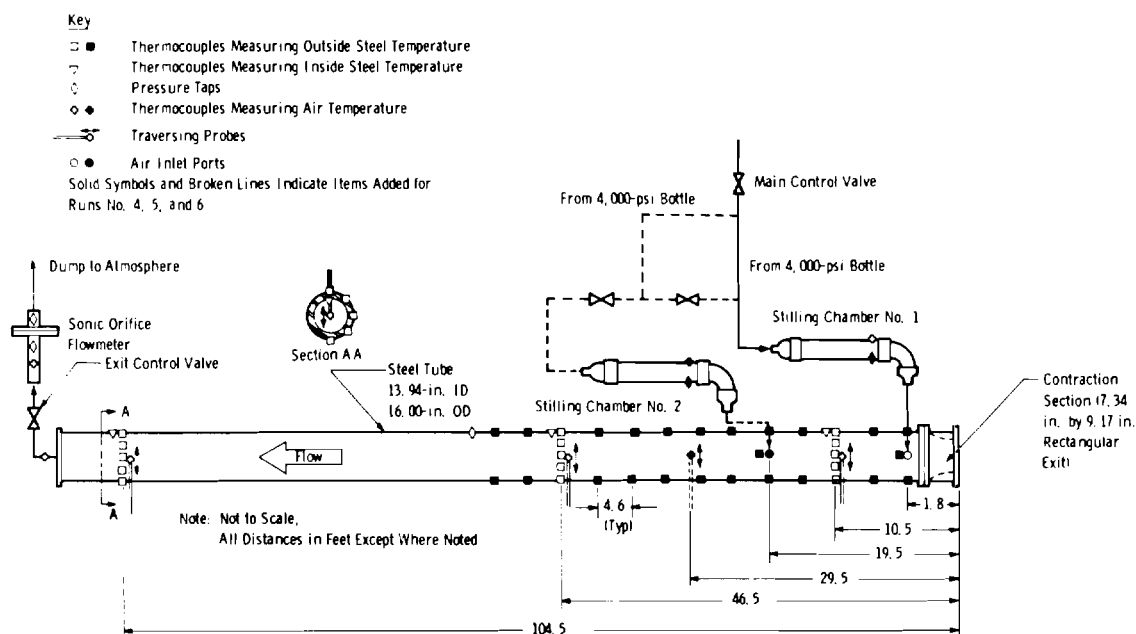


Figure 1. Schematic of experimental apparatus.

The system to handle the cooling air from the 4,000-psi bottle included an automatic control valve which throttled the air to a low enough pressure to prevent choking at the inlet port. Prior to entering the tube, the 3/4-in. supply line was expanded into a 2.5-in.-diam stilling chamber where the stagnation temperature of the inlet air was measured. The air then passed directly from the stilling chamber into the tube through a few inches of 3/4-in. pipe. Air was exhausted from the downstream end of the tube through a control valve and sonic orifice flowmeter (Ref. 2), an arrangement used to control and measure the mass flow rate through the tube. The exhaust line leaving the tube was instrumented with a thermocouple to measure the exit air temperature upstream of the control valve. The flowmeter also contained a thermocouple upstream of the orifice as well as pressure gages on either side of the orifice plate to ensure the pressure drop across the plate was sufficient to keep it choked. Downstream of the meter the air was exhausted to atmosphere. Pressure in the tube was measured with a precision pressure transducer located approximately at the midpoint of the tube. The very low velocities and correspondingly small pressure drops along the tube did not warrant the installation of additional pressure taps along the tube. Since calculations indicated that free convective heat transfer from the outside of the tube was important, the entire tube was wrapped in fiber glass insulation backed with aluminized Mylar[®] to reduce losses. The inlet and outlet plumbing were wrapped with insulation tape.

Three cooling runs were made with this apparatus, and the results indicated the need for more detailed information on the development of circumferential and axial temperature

gradients in the tube as well as the possibility of reducing these gradients with additional inlet ports. To collect this additional temperature gradient data, the tube was further instrumented with thermocouples at eleven additional stations along the tube (black squares in Fig. 1). At each station a thermocouple was attached at the top and bottom of the tube. In addition, a second inlet port and stilling chamber were installed about 15 diameters downstream of the first inlet port. The plumbing, valves, and pressure gages necessary for control of the two inlet ports were also added to the system.

The data collection was performed with a slow speed scanning digital voltmeter which scanned the 25 to 50 channels of thermocouples and pressure taps. The first-line data reduction was performed during the test using a digital computer to convert the voltage printouts to temperatures.

3.0 PROCEDURE

Six separate cooling tests were begun by first pumping the charge tube up to the desired pressure with the exit valve closed. Upon reaching the charge pressure, the inlet and outlet valves were adjusted to produce the desired mass flow rate and hold the charge pressure constant. At intervals from 15 to 30 minutes, readings were taken from all data channels. Measurements were taken from the three air survey probes at five vertical positions by manually sliding the probes up and down. At the conclusion of the test, the flanges capping the ends of the tube were removed to allow the tube to warm up to room temperature for the next test.

On certain individual tests, various special operations were performed. On Run No. 1, following completion of the cooling process, the tube was allowed to stand idle at pressure with no mass flow to determine how rapidly the circumferential and axial temperature gradients in the tube would dissipate. On Run No. 2, this was tried at atmospheric pressure rather than charge pressure. On Run No. 4, the effects of staging on the cooling process were measured. On this run, cooling air was injected through the first air inlet port for several hours until the steel in the region of the inlet approached the inlet air temperature. The first inlet port was then closed and the second one opened (15 diameters downstream) for the remainder of the test.

Sonic orifice calibrations were performed by pumping the tube to a given pressure, shutting off the inlet air, and then dumping the tube through the sonic orifice while measuring pressure and temperature-time histories in the tube and sonic orifice.

4.0 RESULTS

The data to be discussed below were obtained after two levels of data reduction. The first level, performed during the test, consisted primarily of converting the thermocouple voltages to temperatures using either curve-fits of Ref. 3 or curve-fits to the standard tabular data. These temperature-time histories were later converted to heat-transfer coefficients and Nusselt numbers according to the computational procedure discussed in Appendix A. The conditions for each of the six runs are summarized in Table 2.

Table 2. Test Conditions

Run Number	1	2	3	4	5	6
Charge Pressure, psig	400	150	75	150	75	150
Average Mass Flow Rate, lbm/sec	0.41	0.37	0.34	0.33	0.33	0.33
Test Time, Air Flowing, hr	4.9	7.0	5.0	7.5	3.9	3.0
Idle Period at End of Test, hr	0.9 at pressure	1.0 at ambient	0	0	0	0
Inlet Temperature Range, °R	475 to 490	454 to 475	462 to 482	450 to 477	460 to 481	480 to 488
Average Velocity in Charge Tube, ft/sec	0.17	0.40	0.68	0.34	0.65	0.36
Reynolds Number Based on Tube Diameter	39,000	36,000	33,000	33,000	32,000	31,000
Grashof Number Based on Tube Diameter	2×10^{10}	5×10^9	2×10^9	5×10^9	2×10^9	5×10^9
Initial Tube Temperature Range, °R	525 to 529	524 to 531	526 to 529	530 to 536	528 to 530	530 to 534
Final Tube Temperature Range, °R	496 to 515	475 to 503	486 to 517	477 to 507	479 to 522	488 to 522
Prandtl Number	0.68	0.68	0.68	0.69	0.68	0.68

Some of the temperature-time histories from Runs No. 1, 2, and 3 are presented in Figs. 2 through 6. For these first tests, temperature measurements were limited to three axial stations along the length of the tube (Fig. 1) located roughly near the inlet, the midpoint, and the outlet. Tests were conducted at pressures of 400, 150, 75 psig for nominally constant mass flow rates of 0.3 to 0.4 lb/sec. Figure 2 shows how the steel temperature varied during six hours of Run No. 2 (150 psig). As expected, the steel temperature dropped most rapidly near the inlet since this is the region of greater air-steel temperature difference early in the test. The two stations further downstream showed correspondingly lesser slopes since they were cooled by increasingly warmer air. For each station, curves are shown for both the top and bottom outside temperature. At Station 1, there was essentially no difference in temperature between the top and bottom of the tube. At Station 2 there was a marked difference - as great as 10°R at 3.5 hours - and Station 3 showed a significant but lesser difference. The explanation of these experimental results is believed to lie in accounting for the turbulence caused by the inlet jet, which reached velocities of 200 to 300 ft/sec. After presentation of the remaining experimental results, the turbulent mechanism believed responsible will be discussed in more

detail along with an attempt to model these results. One additional curve on Fig. 2 shows how the inlet air temperature varied during the test. The 20°R variation shown here is attributable to variation of the pressure of the air supply, which was nominally 3,500 psig but occasionally dropped below 2,000 psig. The variation of the supply pressure was due to other heavy users of the supply bottle and resulted in varying Joule-Thompson drops in stagnation temperature. The effect of the inlet temperature rise beginning at about one hour can be seen in the slightly lower slope of the steel temperature between two and three hours, and the gradual warming at Station 1 beyond 4.5 hours resulted when the inlet air temperature actually rose above the local steel temperature. With the exception of the top-to-bottom temperature differences, the data shown in Fig. 2 for Run No. 2 may be considered typical of all six runs.

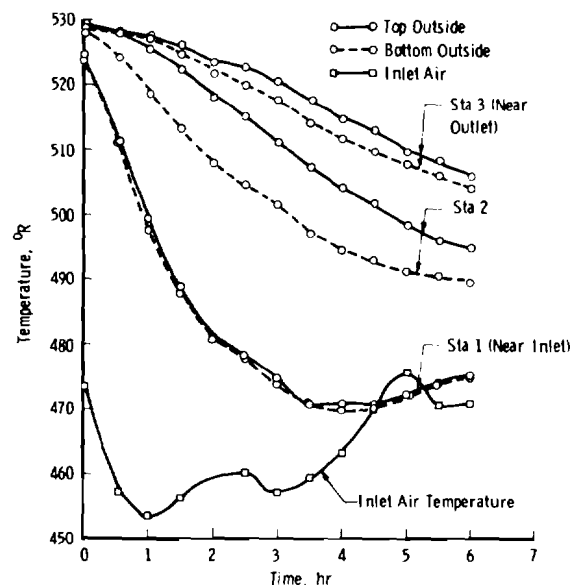
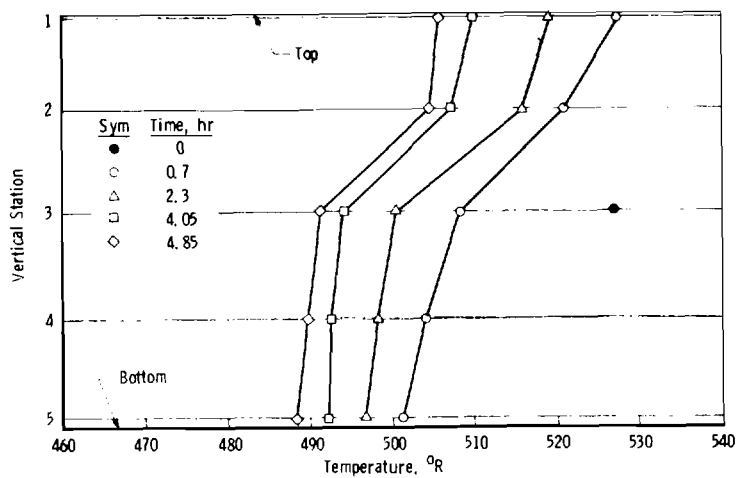
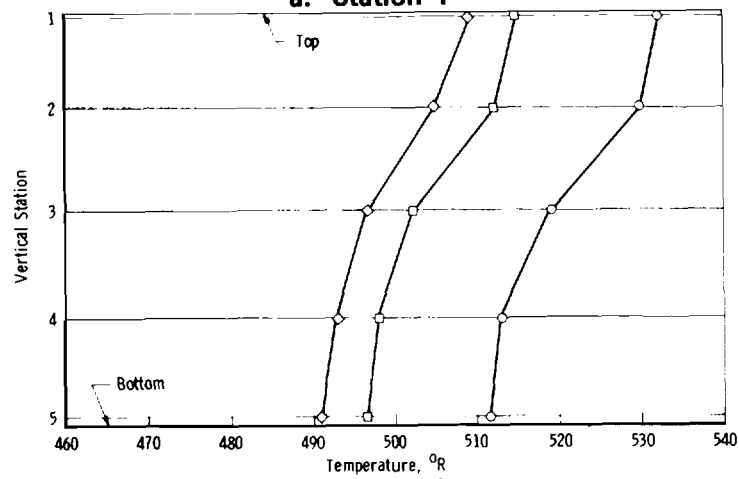


Figure 2. Steel temperature as a function of time for Run No. 2 (150 psig).

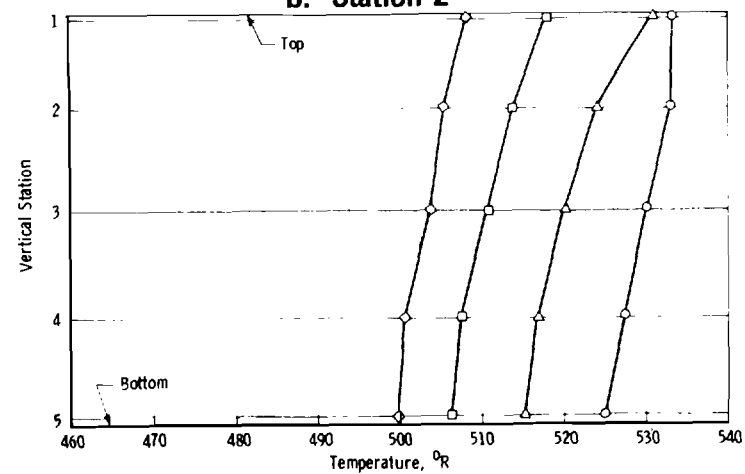
The circumferential temperature difference in the tube is of course due to vertical temperature gradients in the cooling air. Figures 3, 5, and 6 show the data obtained with the sliding air survey probes. Figure 3 compares the vertical gradients at each axial station for Run No. 1 (400 psig). Note that significant gradients occur at all three stations, but that the gradients tend to decrease in the downstream direction. Figure 4 shows similar data for the circumferential steel temperature. Note the large gradients at Stations 1 and 2 during most of the run. The gradients at Station 3 before the two-hour point are small but consider also that little cooling has taken place (the air is relatively warm by the time it reaches Station 3). As Station 3 begins to cool beyond two hours, however,



a. Station 1



b. Station 2



c. Station 3

Figure 3. Air survey temperatures for Run No. 1 (400 psig).

gradients do begin to appear. Figure 5 shows data for 150 psig, and there are marked differences from the 400-psig case. There are essentially no gradients at Station 1 while Station 2 shows heavy stratification and Station 3 somewhat lesser gradients as compared to Fig. 5b. Figure 6 (75 psig) shows no stratification at the first station, slight but temporary stratification at the second, and significant stratification at the third.

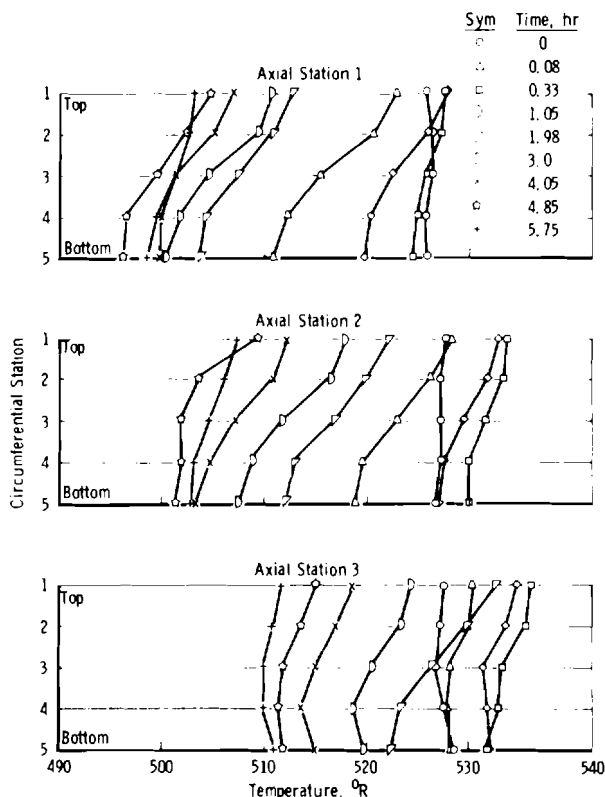
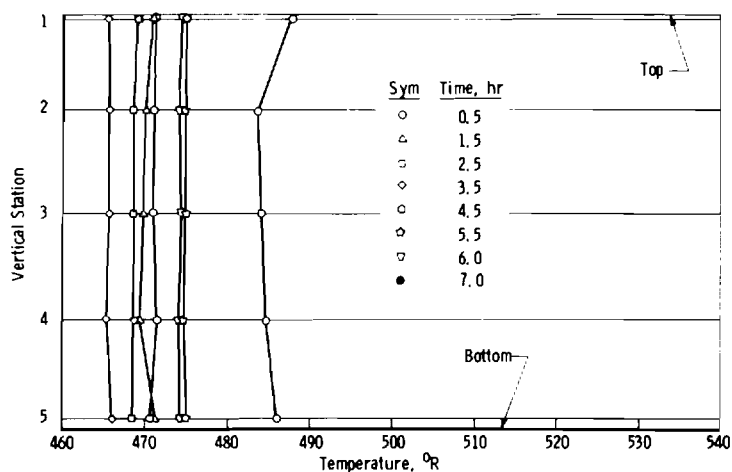
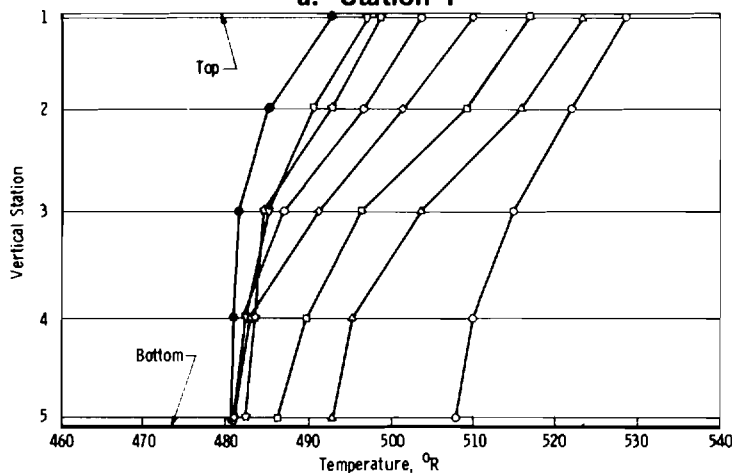


Figure 4. Circumferential steel temperature distribution for Run No. 1 (400 psig).

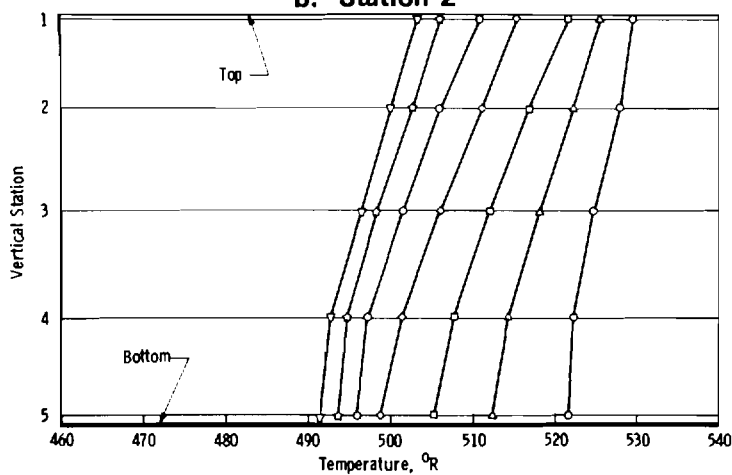
At the completion of Runs No. 1 and 2, after the cooling air had been shut off, the tube was allowed to stand idle for an hour while the gradients dissipated. The idle period following Run No. 1 was at full-charge pressure of 400 psig, while Run No. 2 was at ambient pressure. Figure 7 shows how the top-to-bottom temperature difference in the tube varied during the idle hour at each of the three stations. The gradients were, of course, much larger at the end of Run No. 1 because of the higher operating pressure; by 0.8 hours after shutdown, the gradients had dropped to less than 5°R . Following Run No. 2 the gradients were already less than 5°R but temporarily increased slightly before dissipating, due probably to the sudden loss of the jet turbulence and setting up of a



a. Station 1



b. Station 2



c. Station 3

Figure 5. Air survey temperatures for Run No. 2 (150 psig).

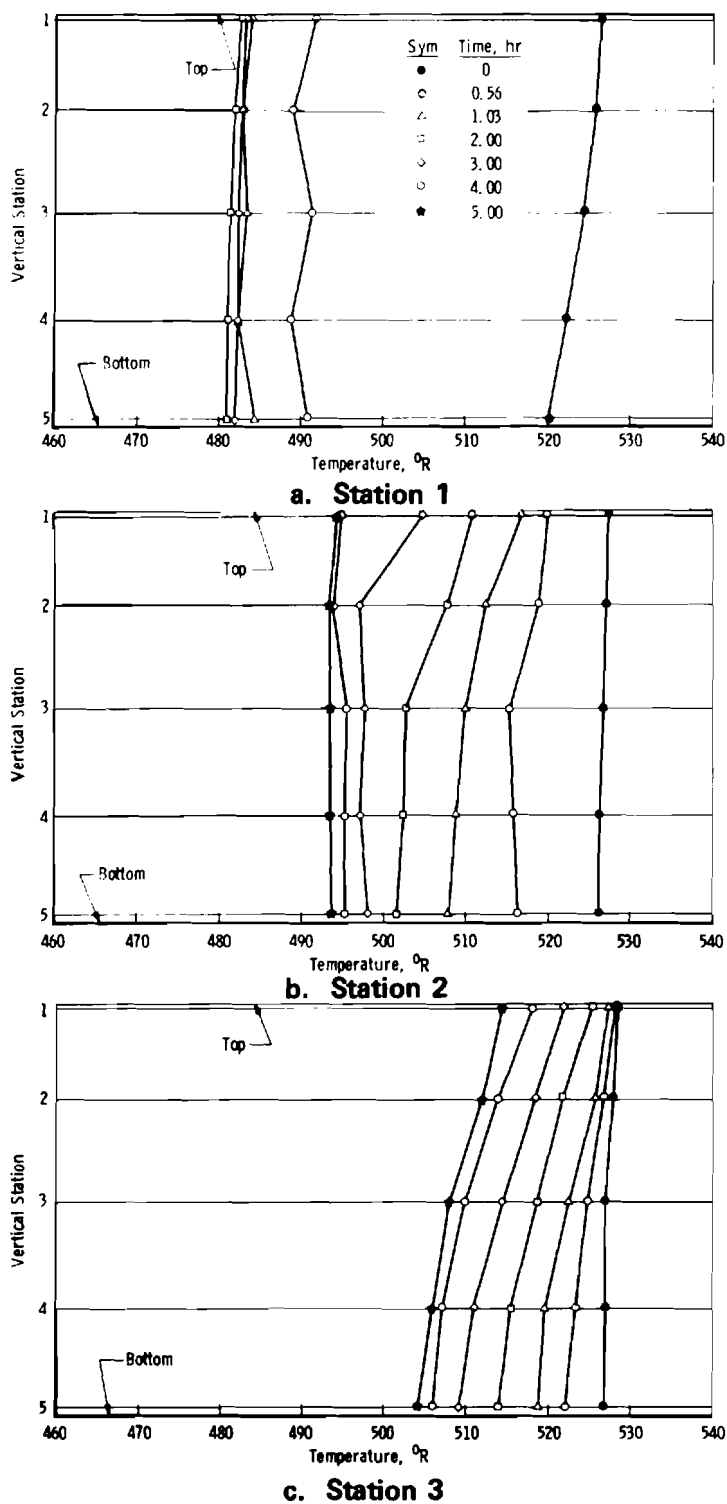


Figure 6. Air survey temperatures for Run No. 3 (75 psig).

strong free convection cycle. The rise in gradients did not appear in the first case because they were already so large and the jet turbulence was of little importance in the high-pressure case.

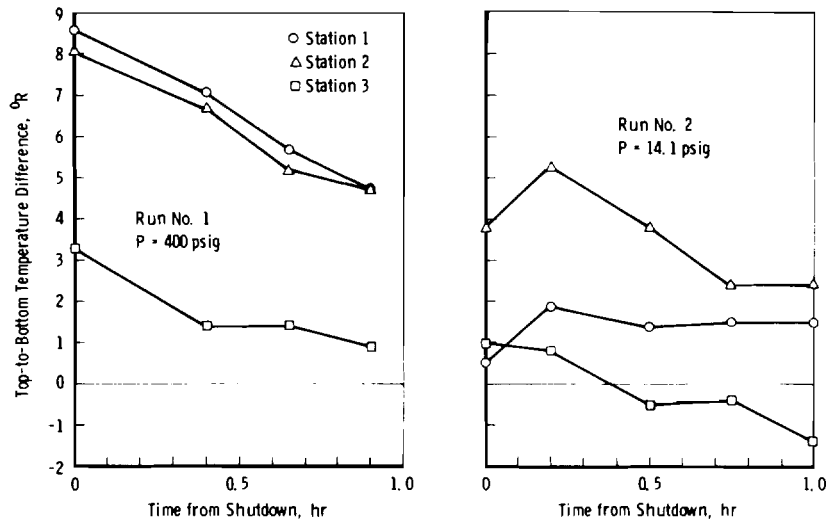


Figure 7. Dissipation of circumferential temperature gradients in tube following shutdown of cooling air.

To refine the results of the first three runs and study the effects of stratification in more detail, three additional runs were made after further instrumenting the tube as explained previously. Figures 8 and 9 show how the top-to-bottom temperature gradients

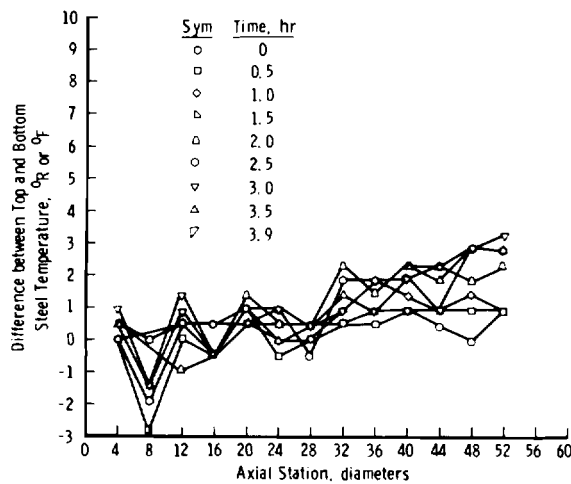


Figure 8. Effect of stratification for Run No. 5 (75 psig).

in the tube varied with time and axial position along the tube. At 75 psig (Fig. 8) the gradients are seen to be essentially zero out to 28 diameters but show a sudden increase from that point on. At twice the pressure (Fig. 9), the small gradients extend only to 24 diameters and then increase much more rapidly from there on. Run No. 4 (150 psig) was performed to measure the effect upon these gradients of moving the inlet jet further downstream once an initial section of the tube had been cooled significantly below ambient. At 5.5 hours into the run, air inlet port No. 1 (Fig. 1) was closed and port No. 2 was opened. Figure 10 shows the large axial temperature gradients in the tube just before

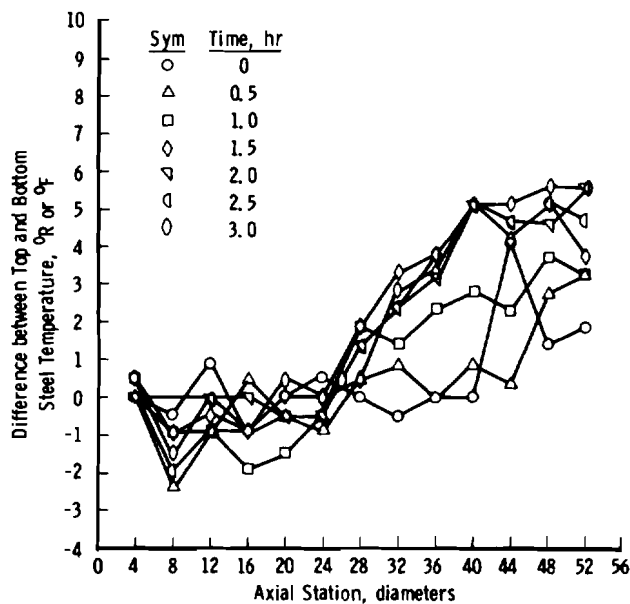


Figure 9. Effect of stratification for Run No. 6 (150 psig).

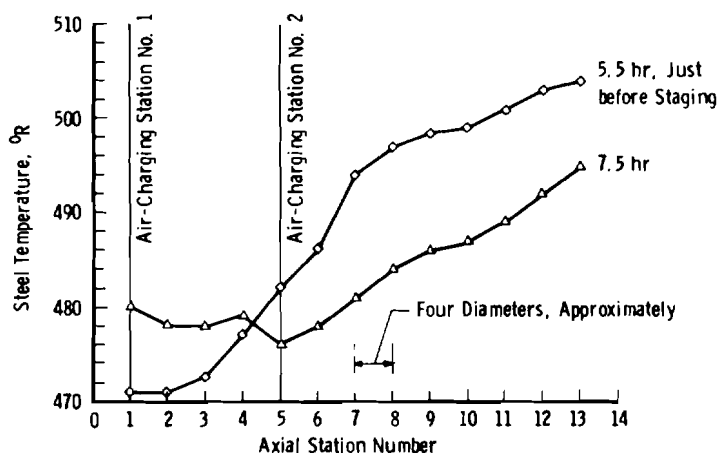


Figure 10. Steel temperature at top of tube versus axial station for Run No. 4 (150 psig) before and after staging.

staging (changing of inlet ports) at 5.5 hours. Two hours later the gradients upstream of the second inlet had essentially washed out. Figure 11 shows a similar effect on the circumferential temperature gradients. Note again the sudden increase in the gradients after a certain distance from the inlet.

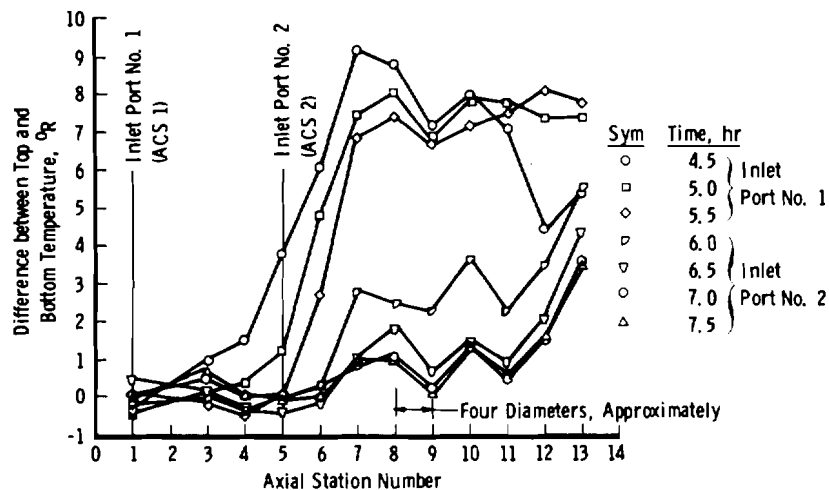


Figure 11. Difference between top and bottom steel temperatures for Run No. 4 (150 psig).

From the temperature-time histories of the air and steel, heat-transfer coefficients along the tube may be computed as outlined in Appendix A. Figure 12 shows the results of this calculation, which accounted for the vertical and circumferential temperature gradients with an averaging technique. Gradients in the radial direction (normal to the tube wall) were shown to be nearly zero by the thermocouples mounted on the inside wall and were therefore ignored in the data reduction. In Fig. 12, the experimental heat-transfer coefficients are shown as scatter bands. The scatter at 88 diameters, for instance, can be charged to the very small air-steel temperature differences which result when the air has been warmed to near the local tube temperature. Thus, when the small net heat transfer, as manifested by the small timewise change in steel temperature, is divided by the air-steel temperature difference, which is also small, the uncertainty in the calculated heat-transfer coefficient becomes somewhat large. The experimental data are compared with three classical Nusselt number relations: the turbulent flat plate boundary layer, the fully developed turbulent pipe, and free convection in an enclosed space (Ref. 4). It is clear that none of the classical relations correlate well with the experimental results, though far downstream free convection gives the closest estimate. In fact, the heat-transfer mechanism occurring in this experiment produced heat-transfer coefficients which are two to five times greater than anything expected from classical theory.

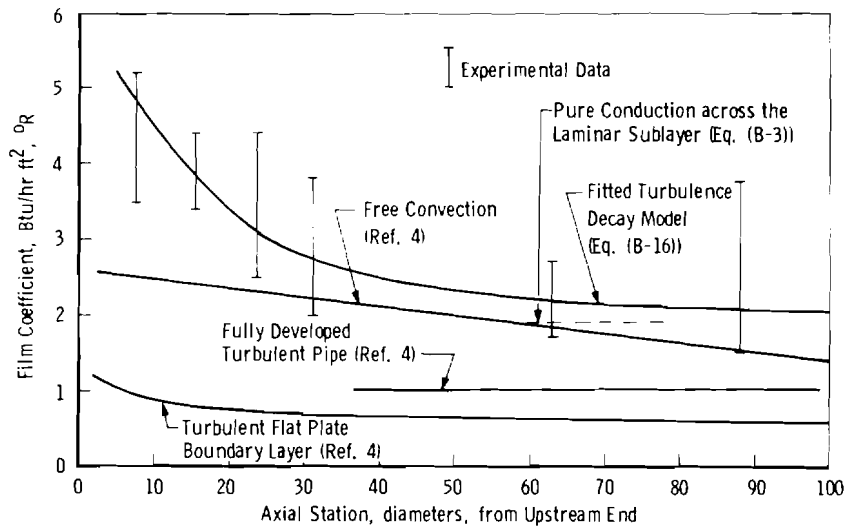


Figure 12. Experimental heat-transfer coefficients compared with classical Nusselt number relations.

In summary, the following experimentally derived facts may be compiled.

1. The flow in the tube stratifies into layers of warmer and cooler air, the degree of stratification depending upon the charge pressure and distance from the inlet.
2. At the lower pressures and sufficiently close to the inlet port, the stratification is essentially zero but seems to grow suddenly at some specific distance from the inlet, also depending upon the pressure.
3. The mechanism responsible for these phenomena produces rates of heat transfer much greater than expected from any classical theory.

5.0 DISCUSSION

The three experimental conclusions listed in the preceding section appear to be logically explainable in the following terms. The inlet jet (200 to 300 ft/sec) sets up a relatively intense turbulence in the upstream portion of the tube. This turbulence immediately begins to decay in intensity through viscous dissipation and is simultaneously convected downstream by the bulk velocity required by the net mass flow rate through the tube. Nearer the inlet, the turbulence is sufficiently intense to prevent development of either a regular free convection flow or a boundary layer. Further downstream, the turbulence eventually decays to the point where it no longer has sufficient intensity to

prevent buoyant forces from inducing stratification of the flow into warm and cold layers. Simultaneously with the decay and convection of the turbulence, an increasing amount of air becomes heated above the inlet temperature, gradually strengthening the importance of buoyancy relative to the turbulence as the warmed masses of air are convected downstream. The effect of the turbulence on the heat-transfer process is to prevent the development of any form of boundary layer and to cycle much colder air within a distance from the wall much less than that of a boundary-layer thickness. As the turbulence decays and buoyancy increases, free convection gradually takes over as the dominant heat-transfer process with stratification as the consequence.

In an attempt to correlate this proposed flow model with the experimental results, a simplified mathematical model has been developed in Appendix B. The model treats the heat-transfer process as one of pure conduction across a thin layer of fluid with a thickness of the order of a laminar sublayer reduced in thickness by the jet turbulence. Comparison of the laminar sublayer thickness for a turbulent pipe flow not disrupted by a jet with a reduced sublayer needed to produce the experimental heat-transfer coefficients allows an approximate estimate of the turbulent intensity and its variation with distance from the inlet. A second part of the model postulates that the onset of stratification may be correlated with axial variation of the ratio of the turbulent energy to the buoyant energy and that when this energy ratio falls below a critical value, stratification begins. The resulting quantitative model predicts that the energy ratio at any given axial station is inversely proportional to the fourth root of the pressure, which agrees roughly with the points (on Figs. 8 and 9) at which stratification occurs.

The model described above is not the only possible explanation of the experimental results, and two alternate hypotheses were considered. The first of the two ideas which received considerable attention was an explanation of the onset of stratification in terms of a growing thermal boundary layer. The essential idea was that a warm boundary layer grew on the wall and merged inward toward a more or less uniform cold core. When a sufficient mass of warmed air had accumulated within the thermal layer, buoyant forces eventually broke up the layer and allowed the unevenly heated air to stratify into hot and cold layers. This idea was eventually rejected because the air temperature distributions measured with the sliding probes showed no signs of a thermal boundary layer. A second idea suggested that the elevated heat-transfer rates might be attributable to the roughness of the inside of the tube. Accordingly, the roughness of the tube was measured and found to be about 0.0015 in. The resulting roughness-to-tube diameter ratio indicated the tube was essentially smooth. Thus, no significant increase in heat transfer resulted from a roughness correction. It therefore appears that the most feasible model of the heat-transfer process studied here is that of decaying jet turbulence opposing buoyant effects as discussed in Appendix B.

Several potentially useful relations have been obtained from correlating the proposed model with experimental data. The heat-transfer rate as a function of position in the tube may be computed from the following empirical equation, developed in Appendix B

$$Nu_D(\tilde{x}) = 0.020 [Re_D (1 + 0.0074 \epsilon e^{-0.057 \tilde{x}})]^{0.875} Pr^{0.4}$$

which was determined from data covering a diameter Reynolds number range of 32,000 to 39,000 and axial position of $0 \leq \tilde{x} \leq 88$ diameters. The Prandtl number varied little from 0.7, and the tube-to-jet area ratio (ϵ) was 353. The equation is plotted in Fig. 12 with the experimental data and the other more conventional theories discussed earlier. It is clear that this relation correlates the data better than the classical theories. As might be expected from the mechanism of decaying turbulence, the proposed model is in better agreement with the free convection process.

An energy ratio correlation equation was developed in Appendix B (Eq. (B-22)). By evaluating the known parameter, Eq. (B-22)) can be rearranged to give the approximate location of the last unstratified station.

$$\tilde{x}_{crit} = 17 \ln \frac{\epsilon Re_D}{Gr_D^{0.564}} - 38$$

where the critical energy ratio was taken as 30 from Fig. B-2 and the Grashof number of the data base ranged from 2×10^9 to 2×10^{10} . Uniform cooling of a tube of length greater than x_{crit} can be achieved by spacing multiple inlet ports at intervals along the tube at spacings of about x_{crit} and cooling the tube in stages. The correlation equation also suggests the unstratified length of tube may be extended by increasing the jet turbulence (reducing the jet flow area), though this approach is practically limited by the jet Mach number.

6.0 SUMMARY OF RESULTS

Heat-transfer rates measured in a long, slender, externally insulated pipe having forced convective internal cooling have been found to be much greater than that expected from classical theories. In addition, significant thermal stratification has been measured at various distances from the inlet port, apparently depending upon the charge pressure. Since no conventional model was found to satisfactorily explain the observed phenomena, a model was developed from the basic idea of decaying turbulence initially produced by the inlet jet. In this model the turbulence not only elevates the heat-transfer rate near the inlet but also delays the onset of thermal stratification. Decay of the turbulence, however, eventually allows free convection to dominate. The axial location where stratification begins

(\tilde{x}_{crit}) has been correlated with a critical value of the turbulent-to-buoyant kinetic energy ratio. The gross effects of stratification and its dependence upon pressure have been verified from the present experimental results, but confirmation and refinement of the detailed explanation must be based upon more elaborate testing, including measurement of turbulence along the tube and measurement of the temperature distribution over the entire cross section of the tube. The results obtained so far, however, do allow some estimate of the effect of the jet upon the heat-transfer rate and upon the length of tube that may be uniformly cooled by depending upon jet turbulence to prevent free convection. In addition, it appears feasible to uniformly cool longer lengths by using multiple inlet ports to cool the tube in stages. The distance between stages should be about \tilde{x}_{crit} .

REFERENCES

1. Starr, R. F. and Schueler, C. J. "Experimental Studies of a Ludwig Tube High Reynolds Number Transonic Tunnel." AIAA Paper No. 73-212, 1973, Also AEDC-TR-73-168 (AD771646), December 1973.
2. Kastner, L. J., Williams, T. J., and Sowden, R. A. "Critical-Flow Nozzle Meter and Its Application to the Measurement of Mass Flow Rate in Steady and Pulsating Streams of Gas." Journal of Mechanical Engineering Science, Vol. 6, No. 1, 1964.
3. Benedict, R. P. "Generating Thermocouple Reference Tables. Instruments and Control Systems. January 1974.
4. Ede, A. J. An Introduction to Heat Transfer; Principles and Calculations, Pergamon Press, Oxford, New York, 1967.
5. Rouse, Hunter. Elementary Mechanics of Fluids. John Wiley & Sons, Inc., New York, 1946.
6. Chapman, D. R. "Laminar Mixing of a Compressible Fluid." NACA Report 958, 1950.

APPENDIX A

COMPUTATION OF HEAT-TRANSFER COEFFICIENTS FROM EXPERIMENTAL TEMPERATURE DISTRIBUTIONS

Two methods of computing heat-transfer coefficients were used herein, one based on the time rate of change of steel temperature at a given axial location along the tube and the other based on the axial variation of the air temperature and the mass flow rate. Consider the first method. Taking as a definition for the heat-transfer coefficient (h) the equation

$$\dot{q} = h\Delta\theta_{as} \quad (A-1)$$

where q is the heat transfer per unit surface area, and $\Delta\theta_{as}$ is the temperature difference between the air and steel, h can be easily determined from the experimental data. For a surface area A ,

$$\dot{q} = \dot{Q}/A \quad (A-2)$$

The energy equation for a control mass of the steel yields

$$Q = M_s C_{p_s} [\theta_s(x,t) - \theta_s(x, t + \Delta t)] \quad (A-3)$$

where M_s is the mass of the steel, C_{p_s} is the specific heat, θ_s is the steel temperature at a given axial position, and t is the time. For a thin walled tube,

$$M_s = \rho_s \pi D \tau \Delta x \quad (A-4)$$

where ρ_s is the steel density, D is the diameter of the charge tube and τ its thickness, and Δx is a short length of tube. Then, dividing Eq. (A-3) through by Δt , noting that $A = \pi D \Delta x$, and combining all these results with the four equations, the following data reduction equation emerges.

$$h(x,t^*) = \frac{\rho_s C_{p_s} \tau [\theta_s(x,t) - \theta_s(x, t + \Delta t)]}{[\theta_s(x,t^*) - \theta_a(x,t^*)] \Delta t} \quad (A-5)$$

where θ_a is the air temperature at a given time and position and $t < t^* < t + \Delta t$. Recall from the experimental data that the steel temperature generally varies circumferentially and the air temperature vertically. To account for this, the temperatures in Eq. (A-5) were computed from weighted averages of all the available data at a given axial location. Both the air and steel temperatures at the extreme top and bottom of the tube were weighted 0.5 while all others were weighted 1.0. Another question arose concerning circumferential and axial conduction within the tube, since these possibilities are not included in the

energy equation (A-3). A manual calculation at the most extreme axial temperature differences indicated that conduction along the tube was negligible compared to the heat flux across the film. On the other hand, circumferential conduction was found to be significant, and a precise accounting was worked out for the energy equation. However, it turned out that the correction had no net effect upon the weighted average steel temperature and thus did not change the experimental heat-transfer coefficients computed without the correction.

In the second method, the heat-transfer coefficient was computed on the basis of air temperature variation. The integral energy equation for a control volume can be reduced to

$$\dot{Q} = \dot{m} C_{p_a} [\theta_a(x_2, t) - \theta_a(x_1, t)] \quad (A-6)$$

where x_1 and x_2 are the inlet and outlet positions on the control volume, C_{p_a} is the specific heat of air, and \dot{m} is the mass flow rate. Taking the area equal to $\pi D(x_2 - x_1)$ and combining Eqs. (A-1), (A-2), and (A-6) produces

$$h(x^*, t) = \frac{\dot{m} C_{p_a} [\theta_a(x_2, t) - \theta_a(x_1, t)]}{\pi D(x_2 - x_1) [\theta_s(x^*, t) - \theta_a(x^*, t)]} \quad (A-7)$$

where $x_1 < x^* < x_2$. For computational purposes x^* and t^* were taken as the midpoint of the space and time intervals.

APPENDIX B

PARTIAL MODEL OF THE HEAT-TRANSFER PROCESS

Several attempts were made to model the heat-transfer process in terms of relations which would reduce to classical theories. Three classical theories are shown in Figure 12. Relations are shown for a turbulent flat plate boundary layer; forced convection in fully developed, turbulent pipe flow; and turbulent free convection inside a sphere. Free convection gives the closest approximation to the experimental data but is probably not sufficient to explain the heat-transfer process encountered. Models in terms of flat plate boundary layers and fully developed pipes modified by the inclusion of decaying jet turbulence were considered, but they were both rejected because the experimental profiles did not exhibit boundary-layer properties. The model finally settled upon was derived from a suggestion that the effect of the jet turbulence is to reduce the boundary-layer thickness. It was thus hypothesized that the jet turbulence reduced the boundary layer to essentially a laminar sublayer so that the heat-transfer process became one of pure conduction across the layer with a relatively large temperature gradient varying from the wall temperature to the bulk fluid temperature over the thickness of the sublayer. Thus, from the one-dimensional Fourier equation for pure conduction,

$$\dot{q} = K_a \frac{\partial \theta_a}{\partial y} \quad (\text{B-1})$$

where y is the direction normal to the tunnel wall, and from Eq. (A-1) the heat-transfer coefficient may be written as

$$h = \frac{K_a}{\delta} \quad (\text{B-2})$$

where δ is the local sublayer thickness. This result assumes

$$\frac{\partial \theta_a}{\partial y} = \frac{\Delta \theta_{as}}{\delta} \quad (\text{B-3})$$

The following equation adequately describes the laminar sublayer thickness for fully developed pipe flow

$$\delta = \frac{32.8 D}{Re_D \sqrt{f}} \quad (\text{B-4})$$

where f is the friction factor given by

$$f = \frac{0.316}{Re_D^{1/4}}, \quad Re_D > 2,000 \quad (\text{B-5})$$

(see Ref. 5). Calculations based on these equations give film coefficients consistent with the experimental data not too near the inlet port (see Fig. 12).

Near the inlet port where the jet turbulence is relatively intense, the sublayer is hypothesized to be of reduced thickness δ' due to a local turbulence of magnitude u' . The Reynolds number in Eqs. (B-4) and (B-5) is thus written as

$$\text{Re}'_D \equiv \frac{\rho(u + u') D}{\mu} \quad (\text{B-6})$$

where u is the local bulk velocity. Another more convenient form is

$$\text{Re}'_D = \text{Re}_D \left(1 + \frac{u'}{u} \right) \quad (\text{B-7})$$

Combining Eqs. (B-4), (B-5), and (B-7) produces

$$\frac{\delta}{\delta'} = \frac{58.3 h D}{K_a \text{Re}_D^{0.875}} \quad (\text{B-8})$$

Use of the experimental heat-transfer coefficients in Eq. (B-8) then gives the ratio of the usual sublayer thickness to that suggested by the elevated heat-transfer rate. Further, from the above equations is it possible to write

$$\frac{u'}{u} = \left(\frac{\delta}{\delta'} \right)^{1.14} - 1 \quad (\text{B-9})$$

which gives an experimental estimate of the turbulent intensity.

The above equations along with classical Nusselt number relations were programmed for computer processing of the experimental data. The statistical distribution of the u'/u data was then examined. Figure B-1 shows the data plotted versus axial distance from the inlet port. The decay of the turbulence was correlated with distance from the inlet with the relation

$$\frac{u'}{u} = 2.6 e^{-0.57 \tilde{x}} \quad (\text{B-10})$$

where \tilde{x} is the nondimensional distance x/D . Correlations with powers of time, such as for an isotropic turbulence, were examined but failed to correlate the data as well as Eq. (B-10). In an effort to establish the dependence of u'/u on the velocity of the inlet jet, the one-dimensional continuity equation between the jet and some uniform station along the large tube was invoked.

$$\rho_j u_j A_j = \rho u A \quad (\text{B-11})$$

For incompressible flow

$$\frac{u_j}{u} = \frac{A}{A_j} \equiv \epsilon \quad (\text{B-12})$$

where the j subscript refers to the jet and ϵ is the area ratio. Assuming then that

$$\frac{u'}{u} = \frac{u_j}{u} \quad (\text{B-13})$$

at $x/D = 0$ so that the constant 2.6 in Eq. (B-10) actually should be written as constant times ϵ , the dependence on the diameter of the charging port appears as

$$\frac{u'}{u} = 0.0074 \epsilon e^{-0.057 \tilde{x}} \quad (\text{B-14})$$

Finally, defining a Nusselt number based on diameter as

$$\text{Nu}_D = \left(\frac{hD}{K_a} \right) \quad (\text{B-15})$$

and using Eq. (B-14) along with the previous sublayer equations, the following Nusselt number relation is obtained.

$$\text{Nu}_D = 0.020 [\text{Re}_D (1 + 0.0074 \epsilon e^{-0.057 \tilde{x}})]^{0.875} \text{Pr}^{0.4} \quad (\text{B-16})$$

To obtain this relation, $\text{Pr}^{0.4}$ (for $\text{Pr} = 0.68$, the experimental Prandtl number) was extracted from the numerical constant in order to compare this equation with the familiar relation for a fully developed turbulent pipe (Ref. 4).

$$\text{Nu}_D = 0.023 \text{Re}_D^{0.8} \text{Pr}^{0.4}$$

The multiplicative constants are comparable in the two relations, but the larger exponent of Re_D in Eq. (B-16) reflects the fact that far downstream the heat-transfer rate of this experiment never decays back to that of a classical fully developed pipe flow, the reason being the eventual domination by free convection. Since the asymptotic value of Eq. (B-16) for large \tilde{x} should, therefore, be a function of the strength of the free convection, the relation must be considered deficient for its lack of dependence upon Grashof number. This obvious extension was not attempted because of the narrow range of Grashof number covered by the experimental data. The relation given by Eq. (B-16) is shown in Fig. 12 with the experimental data from which it was derived.

Before proceeding, it should be understood that the replacement of Re_D by an effective turbulent Reynolds number Re'_D in Eq. (B-4) to obtain a relation for δ' , the effective sublayer thickness in the presence of turbulence, is not rigorous because such

an application of Eq. (B-4) is probably not consistent with the logic behind its classical development. However, note from Eq. (B-4) that increasing the Reynolds number decreases the thickness of the laminar sublayer, a result which would increase the heat-transfer rate for a given temperature difference across the layer. Since this agrees qualitatively with the experiment, it is suggested that the jet turbulence increases the effective Reynolds number. A second point to consider is that in Eq. (B-9) the relative turbulence-induced change in the layer thickness depends not on u' but on the ratio of the turbulent intensity to the local bulk velocity through the tube. For the nominally constant mass flow rates of the experiments, the jet-to-bulk velocity ratio is also nominally constant, according to the assumptions inherent in Eq. (B-11). The logical conclusion, given in these two points, is that the heat-transfer rate should not vary significantly from experiment to experiment (varying only pressure and not mass flow rate). This is consistent with the experiment because within the scatter bands of Fig. 12, no consistent variation with pressure was observed (changing the pressure changes u and u_j but not u_j/u according to continuity). Thus the expedient, but nonrigorous, substitution is justified because it is qualitatively consistent with experimental observation. Obviously, the model to this point would be much stronger if an experimental confirmation of the dependence of the laminar sublayer thickness on free-stream turbulence were available.

Besides the heat-transfer model just described, further data analysis was performed in an effort to understand the stratification in the air temperature, which was manifested in terms of circumferential gradients in the steel temperature. The resulting model has evolved into the following form.

From the experimental data the following facts have been established.

1. Circumferential temperature gradients appear in the steel only when the air has stratified into hot and cold layers at the top and bottom of the charge tube.
2. The onset as well as the rate of increase of stratification is delayed more and more as the pressure is lowered.

Stratification - vertical temperature gradients - is associated with density gradients: hot air rises while cool air falls. But stratification does not occur as long as there is sufficient turbulence to prevent it. It is therefore suggested that the onset of stratification can be correlated with an energy ratio (er) equal to the turbulent kinetic energy divided by the buoyant kinetic energy.

$$er = \left(\frac{u'}{u_b} \right)^2 \quad (B-17)$$

When the jet turbulence has decayed sufficiently, a small, warm lump of fluid with velocity u_b manages to retain its identity long enough to migrate to the top of the tube where its higher temperature reduces the heat-transfer rate from that occurring at the bottom of the tube. When a sufficient number of hot lumps survive the migration time, gradients in the steel begin to appear. The onset of stratification is thus to be correlated with the energy ratio becoming small enough, say less than er_{crit} .

To compute er from experimental data, Eq. (B-14) was used for the numerator of Eq. (B-17). The buoyant velocity u_b was computed by equating the buoyant force on an element of fluid with the drag produced at the terminal velocity allowed by viscous drag. This approach was taken because the unrestrained acceleration attributable to the buoyant force produced absurdly large velocities and short migration times. From Archimedes' principle the buoyant force less the weight of the element may be written as

$$F_b = (\rho - \rho')g V \quad (B-18)$$

where V is the volume of the element, ρ' is its density, g is the acceleration of gravity, and ρ is the density of the surrounding fluid. The drag on the element can be written as

$$F_D = \frac{1}{2} C_D \rho u_b^2 A \quad (B-19)$$

where C_D is a drag coefficient and A is the projected area of the element. The use of Eq. (B-19), which represents drag on a rigid body, requires further discussion. An alternate assumption would be to represent the drag in terms of a viscous shear layer developing between the element and the surrounding fluid (a "nondiscrete" element approach). Such an assumption could take the form of

$$F_D = \mu u_b A/nd \quad (B-19a)$$

where nd represents the thickness of the shear layer. Underlying the choice between Eq. (B-19) and (B-19a) is the question of whether the elements really are discrete. If Eq. (B-19a) is the appropriate model, then the heated element must be losing significant mass to its surroundings via the shear layer and is not discrete. If, however, Eq. (B-19) is more appropriate, then the shear layer is very steep and approximates a more or less solid boundary, a discrete mass. Obviously, neither equation can rigorously represent the entire model. In defense of the discrete model, however, it can be said that the driving force (buoyancy, which is really a body force) acts uniformly on all portions of the element to make them move together. But the basic logic of the discrete assumption is that if the heated elements do not remain sufficiently discrete for a significant duration of time

so as to transport vertically a significant mass of heated air, then classical free convection would not occur. Proceeding with the discrete element theory, some decision on geometry of the element must be made. The approach taken here has been to idealize the element as a discrete piece of fluid of constant geometry - namely, a sphere of diameter d - for which $A = \pi d^2$ and $V = 1/6\pi d^3$. With these relations and the ideal gas law used in the relation resulting from equating F_b and F_D , the following equation emerges.

$$\frac{u_b}{u} = 0.31 \frac{Gr_D^{0.564}}{Re_D} \left(\frac{d}{D}\right)^{0.69} \quad (B-20)$$

where $C_D = 2.67 Re_D^{0.288}$ was fitted to the drag coefficient for a sphere (Ref. 5). Here, Gr_D is the Grashof number defined as

$$Gr_D = \frac{\rho^2 g D^3 \Delta\theta}{\mu^2 \theta} \quad (B-21)$$

and d/D is the ratio of the element size to the tube size, clearly a variable quantity since any hot element formed would dissipate heat and be gradually reduced in size by shear stresses. However, to adopt some hopefully typical value, d/D was taken to be of the order of $\delta - \delta'$, the portion of the laminar sublayer torn away by the turbulence. This calculation gave an estimate of $d/D = 0.01$, which produced reasonable terminal velocities u_b and corresponding migration times. Finally, substitution of Eqs. (B-14) and (B-20) in the definition of the energy ratio Eq. (B-17) yields

$$er = \left(\frac{0.024 \epsilon Re_D e^{-0.057 \tilde{x}}}{Gr_D^{0.564} (d/D)^{0.69}} \right)^2 \quad (B-22)$$

Figure B-2 shows the energy ratio plotted versus axial station. The computation was made using Re_D and Gr_D computed from experimental data. The bands are spaced \pm one standard deviation and represent scatter in the temperature distribution as well as its time-wise variation. The parallelograms locate the last unstratified stations within the distance of two succeeding measurement locations. No location is shown for the 400-psig case because the flow was already heavily stratified as the first measurement location at 7.5 diameters. The value of er_{crit} in Fig. B-2 would appear to be nominally of order 10^2 . The model thus suggests that stratification begins when the energy ratio drops below this value.

An approximate test of Eq. (B-22) may be performed by noting that

$$er \propto p^{-1/4} e^{-0.114 \tilde{x}} \quad (B-23)$$

since $Re_D \propto \rho$ and $Gr_D \propto \rho^2$ while $\rho \propto P$. Taking the natural log of Eq. (B-23) and evaluating at two sets of conditions for a constant energy ratio produces

$$\tilde{x}_2 - \tilde{x}_1 = 2.2 \ln \frac{\rho_1}{\rho_2} \quad (\text{B-24})$$

which is the difference in axial location at which stratification should occur. Comparing the 150-psig case with 75 psig yields a difference of about two diameters while comparing Figs. 7 and 8 yields four diameters, nominally the same result considering the crudeness of the model.

It is important to note at this point, should the fact have been obscured by all the detail, that neither the agreement between the model and the experimental stratification point nor the agreement in Fig. 12 between the heat-transfer model and the data provides a sufficient verification of the proposed model. The comparison does illustrate that the model exhibits the gross level trends of the data, but the degree of agreement is indicative only of the correctness of the calculations to determine the model's constants from the data.

In summary, a model of the heat-transfer process and stratification development has been established from the idea of jet turbulence opposing buoyancy. The obvious weak points in the model are the reduced sublayer and the discrete element drag assumptions, as both are based on essentially misused empirical relations. However, in defense of the present modeling effort, it can be said that the original goal of the effort was to obtain some sensible governing equation by carrying through from first principles the gross level effects postulated to be governing the present physical situation. Obviously, improvement of the turbulence-buoyancy model or derivation of a better one would require a considerable amount of further experimental work.

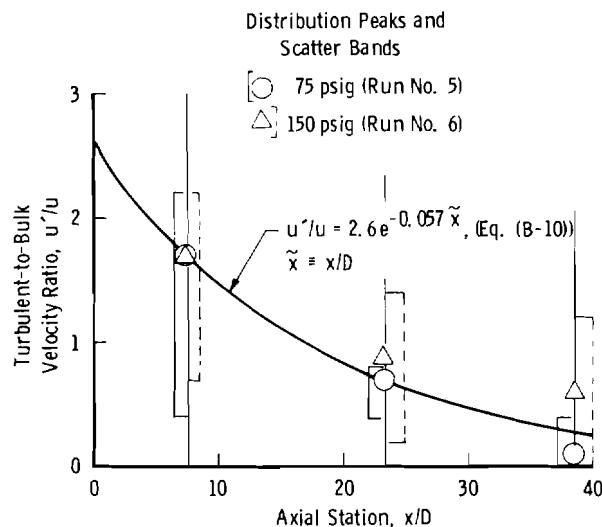


Figure B-1. Decay of jet turbulence.

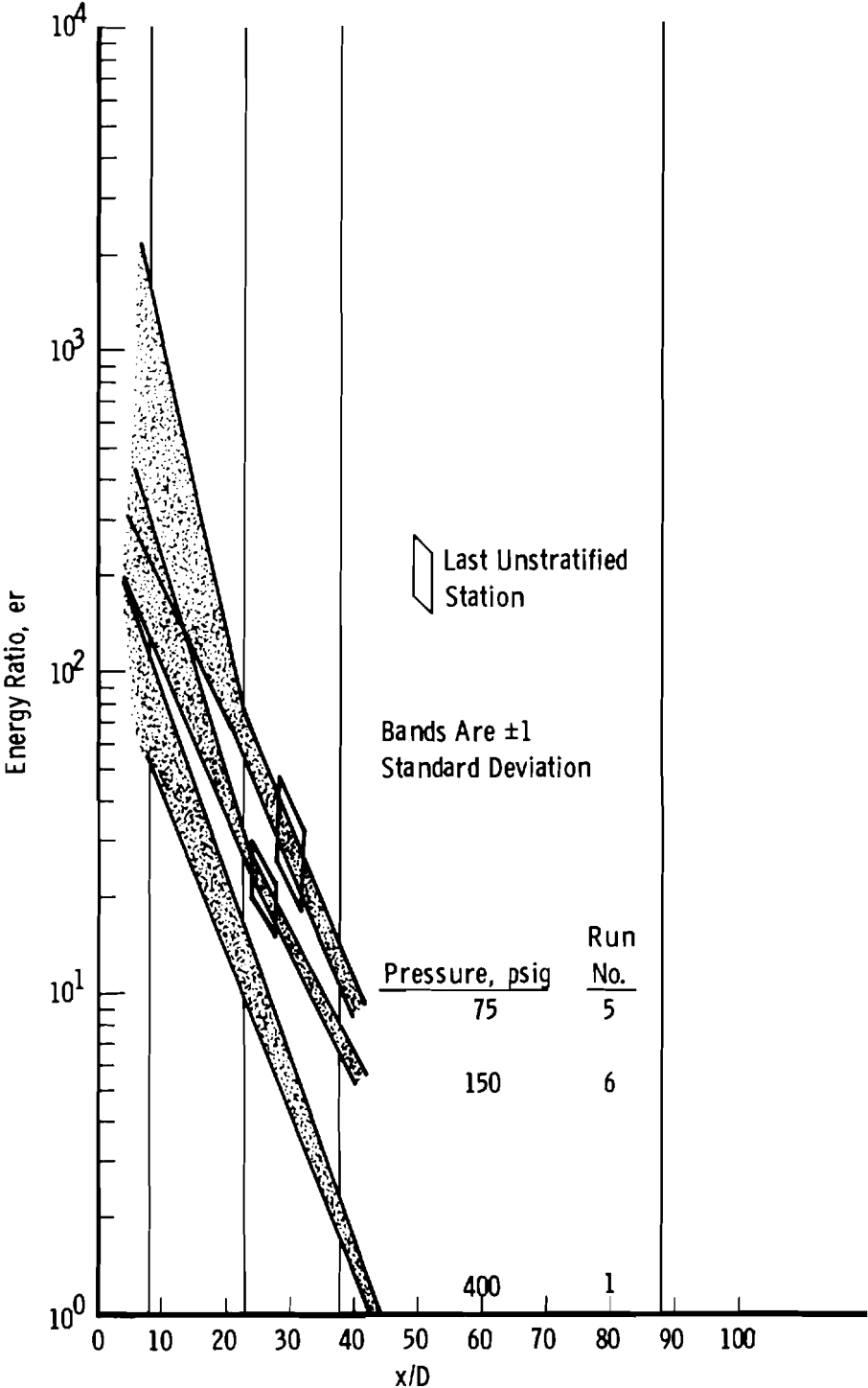


Figure B-2. Energy ratio versus axial station.

NOMENCLATURE

A	Area, cross sectional or surface area depending upon use
C_D	Drag coefficient
C_p	Specific heat at constant pressure
D	Tube inside diameter
d	Element diameter
er	Ratio of turbulent to buoyant kinetic energy
F_b	Buoyant force
F_D	Drag force
f	Friction factor
Gr_D	Grashof number based on tube diameter
g	Acceleration of gravity
h	Heat-transfer coefficient
K	Thermal conductivity
M	Mass
\dot{m}	Mass flow rate
Nu_D	Nusselt number based on diameter
n	Number of elemental diameters in the shear layer
P	Pressure
Pr	Prandtl number, $\mu C_p / K$
Q	Net heat transferred (not heat-transfer rate)
\dot{Q}	Heat-transfer rate
\dot{q}	Heat-transfer rate per unit area

Re_D	Reynolds number based on tube diameter
Re_d	Reynolds number based on size of the heated element of fluid
t	Time
u	Velocity
V	Volume
x	Axial distance along tube
y	Normal distance from tube wall
δ	Sublayer thickness
ϵ	Area ratio, A/A_j
θ	Temperature
ρ	Mass density
μ	Dynamic viscosity
τ	Tube wall thickness

SUBSCRIPTS

a	Air
b	Buoyant
$crit$	Critical value at which stratification begins
j	Jet
s	Steel (or tube)
as	Air-steel, as in $\Delta\theta_{as}$, the air-steel temperature difference
$1,2$	Initial and final stations of a control volume taken from the tube

SPECIAL SYMBOLS

\sim	(over tilde) Nondimensionalization, as in $\tilde{x} \equiv x/D$
\cdot	(over dot) Time derivative, as in \dot{Q} , the net heat-transfer rate
$*$	Intermediate value, as in $t < t^* < t + \Delta t$
Δ	Increment, as in Δt
$'$	(prime) Turbulent quantity, as in u' , or quantity modified by the presence of turbulence, as in δ' , Re_D' , or ρ'
\propto	Proportional to